Applied Energy 194 (2017) 508–521

Contents lists available at ScienceDirect

Applied Energy

journal homepage: www.elsevier.com/locate/apenergy

# The role of porous metal foam on the unidirectional solidification of saturating fluid for cold storage

Xiaohu Yang [a,b], Shangsheng Feng [b,c], Qunli Zhang [d], Yue Chai [a], Liwen Jin [a,*], Tian Jian Lu [b,c,*]

[a] Group of the Building Energy & Sustainability Technology, School of Human Settlements and Civil Engineering, Xi'an Jiaotong University, Xi'an 710049, China
[b] Moe Key Laboratory for Multifunctional Materials and Structures, Xi'an Jiaotong University, Xi'an 710049, China
[c] State Key Laboratory for Strength and Vibration of Mechanical Structures, Xi'an Jiaotong University, Xi'an 710049, China
[d] Beijing Municipal Key Lab of Heating, Gas Supply, Ventilating and Air Conditioning Engineering, Beijing University of Civil Engineering and Architecture, Xicheng District, Beijing 100044, China

## HIGHLIGHTS

- The solidification evolution was retardant when the metallic ligaments were inner hollow.
- The dominating parameter was found to be relative density for phase change heat transfer.
- For low *Ste* number (0.22), local thermal equilibrium may be safely assumed for convenience.
- Natural convection was found negligible at pore-scale for phase change heat transfer.

## ARTICLE INFO

*Article history:*
Received 20 March 2016
Received in revised form 15 September 2016
Accepted 18 September 2016
Available online 5 October 2016

*Keywords:*
Open-cell foam
Cold storage
Direct numerical simulation
Pore-scale analysis
Analytical model

## ABSTRACT

We conducted analytical, numerical and experimental investigations on solidification of fluid saturated in highly porous metal foams with open cells. Based on pore-scale thermal equilibrium assumption, an analytical extension of the classical Neumann's solution was made to predict phase change heat transfer in PCM-foam composites. To explore the heat transfer mechanisms underlying the phase change process and clarify the role of foam insertion, three-dimensional direct numerical simulations on periodically distributed tetrakaidecahedron cells were carried out. Experimental measurements were performed to validate the analytical model and the numerical method, with good agreement achieved. The phase interface was macroscopically flat via experimental visualization but microscopically irregular via pore-scale simulations. Temperature difference between the saturating PCM and metallic ligaments was negligible, so that local thermal equilibrium and one-equation model were applicable especially at low *Ste* numbers (e.g., 0.22). The present findings provide new insights to cold energy storage design, utilization and economic analysis in HVAC systems.



## 1. Introduction

The energy use is rapidly growing all around the world. The statistical data among a total of 69 countries indicates that there have been marked increases in energy use in developing countries such as China, India, Brazil, Thailand and South Africa [1–3]. For instance, the total primary energy demand for China in 2010 is about 3.2 billion tons of coal equivalent, which is 5.6 times of that in 1978 [4,5]. The increasing trend for energy demand will continue in the near future. It is speculated that the energy demand for China will increase to 6.2 billion tons of coal equivalent in 2050 [6]. Besides this, the energy demand for the new emerging economies in Southeast Asia, Middle East, South America and Africa is also increasing at an alarming rate [6]. Such a rapidly growing demand for energy causes a lot of troubles for the world, such as energy depletion, global warming and environment deterioration [7–9].

Amongst the various demands for energy, HVAC system is now playing an increasingly significant role in the total energy consumption in these days, due to the increasing demand for thermal comfort. It is reported that up to 50% of the building energy and approximately 20% of total energy is consumed by HVAC system in America [9]. On one hand, the energy demand is significantly increasing; on the other hand, there exists severe mismatch of

* Corresponding authors at: Group of the Building Energy & Sustainability Technology, School of Human Settlements and Civil Engineering, Xi'an Jiaotong University, Xi'an 710049, China (L.W. Jin).
*E-mail addresses:* lwjin@xjtu.edu.cn (L. Jin), tjlu@xjtu.edu.cn (T.J. Lu).

http://dx.doi.org/10.1016/j.apenergy.2016.09.050
0306-2619/

**Nomenclature**

*Abbreviation*

| | |
|---|---|
| DF | direct foaming |
| DNS | direct numerical simulation |
| FVM | finite volume method |
| HVAC | heating, ventilation and air conditioning |
| PCM | phase change material |
| RPP | replication of polymeric path |

*Symbols*

| | |
|---|---|
| $A$ | area of side and top wall of container ($m^2$) |
| $c_{pe}$ | effective specific heat of PCM-foam composite (J $kg^{-1}$ - $K^{-1}$) |
| $c_{ps}$ | specific heat of metallic ligaments (W $m^{-1}$ $K^{-1}$) |
| $c_{pf}$ | specific heat of PCM (W $m^{-1}$ $K^{-1}$) |
| $D_1$ | diameter of sphere in square face of tetrakaidecahedron cell (m) |
| $D_2$ | diameter of sphere in hexagon face of tetrakaidecahedron cell (m) |
| $D_3$ | diameter of sphere in the center of tetrakaidecahedron cell (m) |
| $e$ | normalized node size of metal foam |
| $f_s$ | solidification fraction |
| $H$ | total height of fluid-foam composite (m) |
| $k_e$ | effective thermal conductivity of PCM-foam composite (W $m^{-1}$ $K^{-1}$) |
| $k_s$ | thermal conductivity of metallic ligaments (W $m^{-1}$ $K^{-1}$) |
| $k_f$ | thermal conductivity of PCM (W $m^{-1}$ $K^{-1}$) |
| $k_p$ | thermal conductivity of Perspex wall (W $m^{-1}$ $K^{-1}$) |
| $L$ | latent heat of PCM (J $kg^{-1}$) |
| $Q_{loss}$ | heat loss through side walls (W) |
| $q_w$ | bottom heat flux (W·$m^{-2}$) |
| $S(t)$ | solidified layer thickness (m) |
| $T_e$ | evaporating temperature (K) |
| $T_i$ | initial temperature (K) |
| $T_w$ | bottom wall temperature (K) |
| $T_m$ | solidification temperature of PCM (K) |
| $T_{s1}$ | temperature inside container wall (K) |
| $T_{s2}$ | temperature outside container wall (K) |
| $\Delta T$ | temperature difference between PCM and metallic ligaments (K) |
| $t$ | time (s) |
| $t_{full}$ | full solidification time (s) |

*Greek symbols*

| | |
|---|---|
| $\alpha$ | inner hollow ratio |
| $\beta$ | normalized ligament length |
| $\gamma_e$ | effective thermal diffusivity of PCM-foam composite ($m^2$ $s^{-1}$) |
| $\gamma_s$ | thermal diffusivity of metallic ligaments ($m^2$ $s^{-1}$) |
| $\gamma_f$ | thermal diffusivity of PCM ($m^2$ $s^{-1}$) |
| $\lambda$ | positive root of transcendental equation |
| $\varepsilon$ | porosity |
| $\rho^*$ | relative density of foam |
| $\rho_e$ | effective density of PCM-foam composite (kg $m^{-3}$) |
| $\rho_s$ | density of metallic ligaments (kg $m^{-3}$) |
| $\rho_f$ | density of PCM (kg $m^{-3}$) |

*Subscript*

| | |
|---|---|
| $e$ | effective |
| $f$ | saturating fluid |
| $i$ | initial state |
| $m$ | solidification point |
| $s$ | metallic ligaments |
| $w$ | wall |
| 1 | solidified phase |
| 2 | liquid phase |

the energy supply and demand during the daytime and nighttime. Energy (thermal or cold) storage technology is an effective way to balance the mismatch of the energy supply and demand. Particularly, air-conditioning incorporated with cold storage system is showing tremendous potential to both maintain the indoor thermal comfort and balance the mismatch of the energy supply and demand for the countries in tropical climate [10–14]. A commercialized air-conditioning system with cold storage technology (water is utilized as the cold storage medium) is successfully applied in Xi'an Xianyang International Airport, which is demonstrated to improve the overall efficiency of the air-conditioning systems and simultaneously improve the economic efficiency.

For the typical cold storage process, cold is stored and released through phase change materials (PCMs) that undergo a change in phase, e.g., solidification and melting of water/water-ethylene glycol mixture. The cold storage and release process, however, suffers significantly from the relatively low thermal conductivity of commonly applied PCMs [15,16]. To enhance PCM conductivity, a range of techniques have been developed such as adding micro-/nano-scaled particles, fin array and porous matrix into the PCM [11,17]. Compared with the attainable enhancement achieved by adding micro/nano particles, non-moving porous metallic matrix is promising for its low cost, structural controllability and satisfactory thermal enhancement [15,18]. Open-cell metal foams have very good robustness for being incorporated into heat exchangers [19–23]. They can be cut in any shape and sintered with heat transfer plates. Fig. 1 shows two kinds of metal-foam-cored plate and tube heat exchanger in typical engineering applications [24].

The phase change behavior of PCM-foam composite has been intensively investigated. Xiao et al. [15] described in detail how to experimentally prepare a PCM-foam composite. The role played by open-cell copper foam in enhancing the heat transfer performance of a solid/liquid phase change thermal energy storage system was experimentally investigated [25]. It was demonstrated that the presence of copper foam dramatically reduced the time needed for thermal storage. Focusing on the unidirectional solidification behavior of water saturating open-cell metallic foam under constant temperature boundary condition, Feng et al. [26] experimentally found that thermal contact resistance was negligible during freezing. Yang et al. [19] experimentally investigated the solidification behavior of fluid saturated in open-cell metal foams with pore-gradient configurations. They found that the stacked foams with properly designed morphology gradient would reduce more effectively the full solidification time, compared to the single-layered foam with fixed morphology.

While experimental observations were capable of providing benchmark and giving direct demonstration of the evolution history of transient solid-liquid phase interface, numerical method based on volume-averaging theory was often utilized to simulate the solidification/melting processes in metallic foams with open cells. Particular focus has been placed upon on clarifying the effects of local thermal equilibrium and non-equilibrium. Tong et al. [27] numerically examined the enhancement of solidification by inserting aluminum (Al) foam into pure water. Li et al. [28], Mesalhy et al. [29], Yang and Garimella [30], Tian and Zhao [31], and Srivatsa et al. [32] numerically solved the volume-averaging

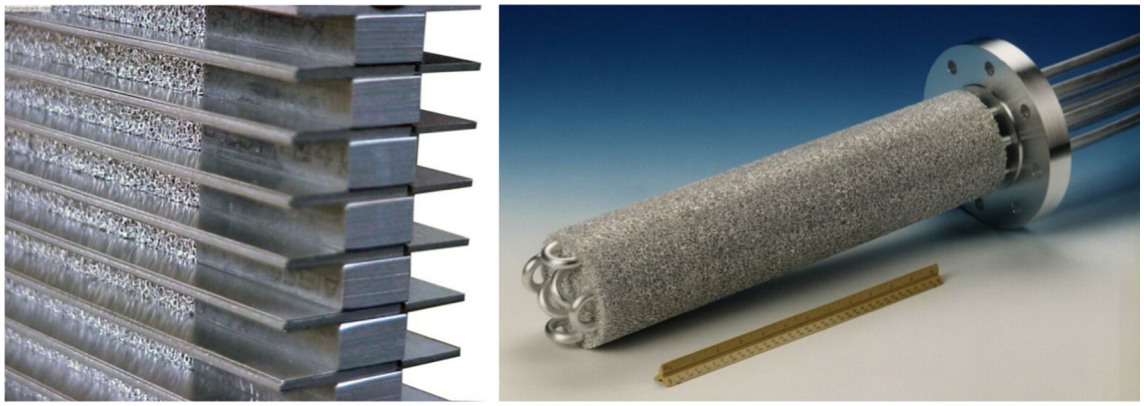


**Fig. 1.** Heat exchangers using open-cell metal foam as the enhancement: (a) plate heat exchanger and (b) tube heat exchanger [24].

equations (two-temperature equations) for phase change in porous metal foams, with non-Darcy effect, local natural convection and thermal non-equilibrium considered.

In addition to volume-averaged simulation, direct numerical simulation (DNS) at pore scale is needed to gain further insights into the phase change phenomena. To this end, Fleming et al. [33] built a column of Kelvin cells saturated with water as the PCM and numerically modeled the solidification of the saturating water. Hu et al. [34,35] numerically compared phase interface propagation in body-centered-cubic lattice embedded with spherical micro-pores and that obtained via volume-averaged simulation. They demonstrated that the DNS could provide new insights into the complicated heat transfer such as three-dimensional (3D) PCM melting front and temperature distribution. Moreover, DNS results were used to extract relevant thermo-physical parameters, e.g., effective thermal conductivity and interstitial heat transfer coefficient [35]. Upon comparing the results obtained by direct simulations on sphere-centered Kelvin cells with those by volume-averaged simulations, Feng et al. [36] suggested that significantly enhanced heat transfer could be achieved by inserting fins into a PCM-foam composite.

Thus far, efforts have been made to investigate the melting behavior of PCM saturated in open-cell metal foams. Only a few investigations have been made into the solidification characteristics for cold storage and the physical details of this phase change process have not been fully understood. Open-cell metal foams are typically fabricated via the replication of polymeric path (RPP) and it is found that the metallic ligaments are inner hollow. The effect of hollow foam ligaments on heat transfer has been so far considered only by numerical simulations based on equivalent thermo-physical properties. The inner hollow foam ligaments have not been thus far considered in either geometric or phase-change point of view for direct numerical simulation. The effect of geometric parameters (e.g., aspect ratio of hollow foam ligaments) on overall phase change heat transfer remains elusive. The three-dimensional (3D) complex topology of open-cell foam has strong influence upon its transport properties, thereby affecting phase change heat transfer in PCM-foam composites. Numerical simulations at pore scale are thus needed to gain better understanding of the physical mechanisms underlying the phase change behavior of such composites. Further, the economic analysis of applicability for open-cell metal foams incorporated into the cold storage system has not been reported in open literature.

The present study aimed to explore the thermo-physics for pore-scale solidification of fluid saturated in open-cell metal foams using a combined analytical, numerical and experimental approach. Special focus was placed upon comparing the influence of thermal equilibrium on solidification with that of non-equilibrium at pore scale. The effects of inner-hollow ratio of foam ligaments on solidification, heat flux and averaged heat transfer coefficient were quantified. The economic features of this technology were also discussed for cold storage.

## 2. Analytical modeling

For a pure substance, Neumann [37] pioneered the mathematical description of its solidification heat transfer. Based on the volume-averaging approach, the PCM-foam composite considered in the present study could be treated as a homogeneous fluid with equivalent thermo-physical properties [38,39]. Consequently, when proper modifications were made, the classical Neumann solution could be employed to predict the phase change heat transfer in PCM-foam composite, as illustrated below.

To simplify the problem, all relevant physical properties of the composite material (in either liquid or solid phase) such as latent heat ($L$), thermal conductivity ($k_s$, $k_f$ and $k_e$), diffusivity ($\gamma_s$, $\gamma_f$ and $\gamma_e$), and specific heat at constant pressure ($c_{ps}$, $c_{pf}$ and $c_{pe}$) were assumed to be invariant in temperature, time, and space.

Fig. 2 depicted schematically the one-dimensional (1D) solidification process in a fluid-foam composite with initial temperature $T_i$. With constant temperature ($T_w < T_i$) imposed on the bottom wall, heat transfer occurred and the fluid next to the wall was solidified once its temperature dropped below the solidification temperature $T_m$. Based on the assumption of local thermal equilibrium and the volume-averaging theory of porous media, the effective thermo-physical properties for such fluid-foam composite could be obtained, as [40]:

$$\rho_e = \rho_s(1-\varepsilon) + \varepsilon\rho_f \tag{1}$$

$$c_{pe} = c_{ps}\frac{\rho_s(1-\varepsilon)}{\rho_s(1-\varepsilon)+\varepsilon\rho_f} + c_{pf}\frac{\varepsilon\rho_f}{\rho_s(1-\varepsilon)+\varepsilon\rho_f} \tag{2}$$

$$k_e = \left(\frac{(1-\varepsilon)k_s}{(1-e+3e/(2\beta))[3(1-e)+3\beta e/2]} + k_f\varepsilon\right)(1-\alpha^2) \tag{3}$$

where $\rho$, $c_p$ and $k$ denoted the density, specific heat and thermal conductivity; subscripts $e$, $s$, $f$ meant "effective", "metallic ligaments" and "fluid"; $\varepsilon$, $e$, $\beta$ and $\alpha$ were foam parameters (porosity, node size, ligament length and inner-hollow ratio), to be determined via pore morphological characterization.

Transient phase interface in the homogenized fluid-foam composite of Fig. 2 could be described using the modified and extended Neumann's solution, as:

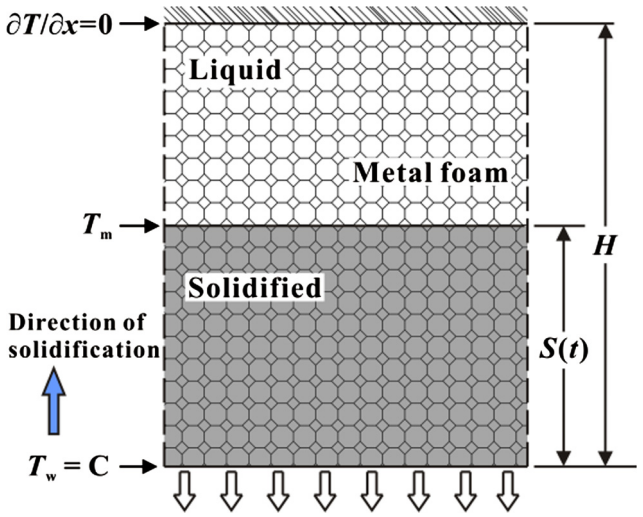


**Fig. 2.** Schematic of one-dimensional solidification of fluid saturated in open-cell foam (initial temperature $T_i$) with constant temperature $T_w$ imposed at bottom wall and thermal insulation on top wall.

$$S(t) = 2\lambda\sqrt{\gamma_e t/H^2} \tag{4}$$

where $S(t)$ was the solidification thickness, $\gamma_e$ was the effective thermal diffusivity to be determined from Eqs. (1)–(3), and $\lambda$ was the positive root of the following transcendental equation:

$$\frac{e^{-\lambda^2}}{erf(\lambda)} - \frac{k_{f2}\sqrt{\gamma_{f1}}(T_i - T)e^{-\lambda^2\gamma_{f1}/\gamma_{f2}}}{k_{f1}\sqrt{\gamma_{f2}}(T - T_w)erfc\left(\lambda\sqrt{\gamma_{f1}/\gamma_{f2}}\right)} = \frac{\lambda L\sqrt{\pi}}{c_{pf1}(T - T_w)} \tag{5}$$

Here, $erf(\lambda)$ and $erfc(\lambda)$ were the Gaussian error functions and subscripts "1" and "2" denoted solidified phase and liquid phase of the saturating fluid, respectively. Once the pore morphological parameters and thermo-physical properties of the fluid-foam composite were determined, the solid-liquid phase interface could be readily predicted using the analytical model presented above.

## 3. Numerical simulation

### 3.1. Foam structure reconstruction

Open-cell metallic foams had been fabricated using two main approaches: direct foaming (DF) and replication of polymeric path (RPP). Different from direct foaming of copper slurry, the RPP approach consists two main steps: (1) fine and smooth copper powder was first deposited on the surface of open-cell polymer foam via electrolytic deposition routine and (2) copper-deposited foam was then processed via vacuum ablation to remove polymer ligaments. Macroscopically, open-cell metallic foams fabricated using the RPP approach had the same 3D topology as that processed via the DF approach. Microscopically, however, they had inner-hollow ligaments due to removing of polymer foam.

In this study, the topology of open-cell foam was modeled as periodically distributed tetrakaidecahedrons to enable 3D numerical simulations. For highly porous open-cell foams, it has been demonstrated that tetrakaidecahedron (as unit cell of foam) originated by Boomsma and Poulikakos [41] was more realistic than other topological structures. Built upon the tetrakaidecahedron unit cell model and the SEM image of typical open-cell metal foam fabricated via the RPP route as shown in Fig. 3(a), we used spheres to cut the original tetrakaidecahedron to form a sphere-cut tetrakaidecahedron, as illustrated in Fig. 3(b). According to previous study [42], the sphere-cut tetrakaidecahedron was actually observable during the foaming process.

The sphere-cut tetrakaidecahedron consisted of six squares, internally cut by a sphere with diameter $D_1$, and eight hexagonal faces, internally cut by a sphere with diameter of $D_2$. Further, the tetrakaidecahedron was centrally cut by a sphere with diameter $D_3$. With global size $a$ and ligament length $t$ (Fig. 3(b)), the porosity and pore window size (pore size) of the sphere-cut tetrakaidecahedron were given by:

$$\varepsilon = \frac{\pi}{4}\left[2\left(3 + 2\sqrt{3}\right)\left(\frac{D_3}{a}\right)^2 - 8\left(\frac{D_3}{a}\right)^3 - (2 + \sqrt{3})\right] \tag{6}$$

$$D_2 = \sqrt{D_3^2 - a^2/12} \tag{7}$$

where $\varepsilon$ represented the fluid saturation fraction of tetrakaidecahedron, namely porosity. However, for foams fabricated via the RPP route, the relative density had the distinct form of:

$$\rho^* = (1 - \varepsilon)(1 - \alpha) \tag{8}$$

where $\alpha$ denoted the inner-hollow ratio of foam ligaments. When $\alpha = 0$, the foam ligaments were no longer hollow.

### 3.2. Direct numerical simulation

With direct numerical simulation (DNS), the assumption of local thermal equilibrium (or non-equilibrium) for heat transfer between metal foam surface and interstitial PCM was no longer needed. To provide the physical basis for direct numerical simulation of phase change heat transfer, $5 \times 6 \times 10$ ($x \times y \times z$) sphere-cut tetrakaidecahedron cells with inner hollow ligaments reconstructed by SOLIDWORKS 2015 were assembled. As shown in Fig. 4, the tetrakaidecahedron cells assembly compared favorably with the real topology of copper-foam used in the present experiments.

To save computing time, only one slice of 10 tetrakaidecahedron cells was chosen as the computational domain due to geometrical symmetry, as illustrated in Fig. 5(a). Direct numerical simulations were then exploited using the finite volume method (FVM) embedded within the commercially available software ANSYS-FLUENT 14.5. Constant temperature thermal boundary and thermal insulation boundary were separately imposed on the bottom and top faces, while the other four faces were symmetrical. Tetrahedron elements were adopted to discretize both the solid and fluid domains; Fig. 5(b).

The thermo-physical properties of both the PCM and metal foam were assumed to be constant, except the density of PCM in liquid phase (water in the present study). Fluid motion in liquid phase was described with the Boussinesq free convection model, with volume expansion due to water solidification neglected. Phase change heat transfer in porous matrix was governed by the continuous and momentum equations in liquid phase and the energy equation for heat transfer in PCM, as:

$$\nabla \cdot \vec{u} = 0 \tag{9}$$

$$\rho_f \frac{\partial \vec{u}}{\partial t} + \rho_f(\vec{u} \cdot \nabla)\vec{u} = -\nabla P + \mu_f \nabla^2 \vec{u} + \rho_f \vec{g}\,\beta(T_f - T_s) + A\vec{u} \tag{10}$$

$$\rho_f c_{pf} \frac{\partial T_f}{\partial t} + \rho_f c_{pf} \vec{u} \cdot \nabla T_f = \nabla \cdot (k_f \nabla T_f) - \rho_f L \frac{\partial f_s}{\partial t} \tag{11}$$

where the coefficient $A$ in Eq. (10) was employed to damp the velocity in solidified phase, given by [43]:

$$A = \frac{C(1 - f_s^2)}{S + f_s^3} \tag{12}$$

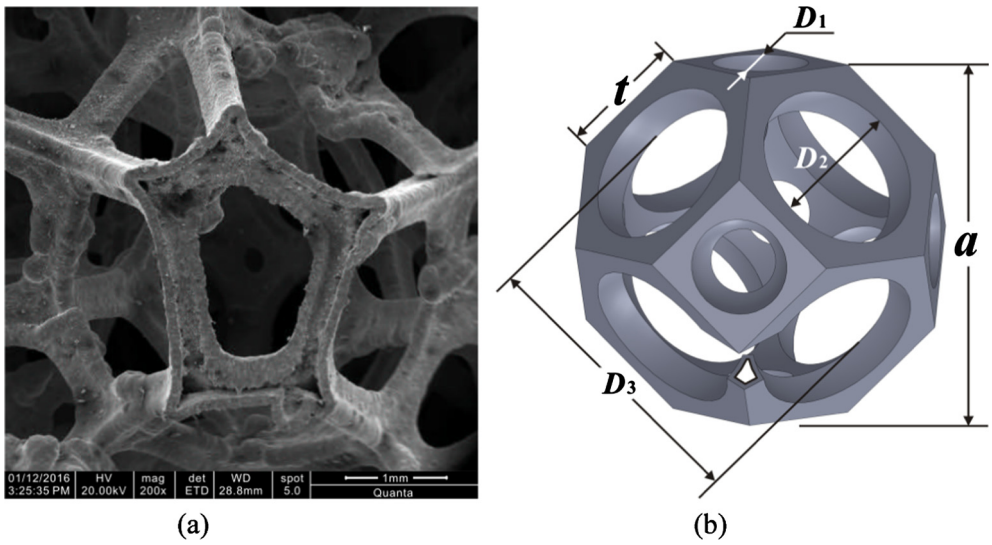


**Fig. 3.** (a) SEM image of open-cell copper foam and (b) idealized tetrakaidecahedron unit cell model.

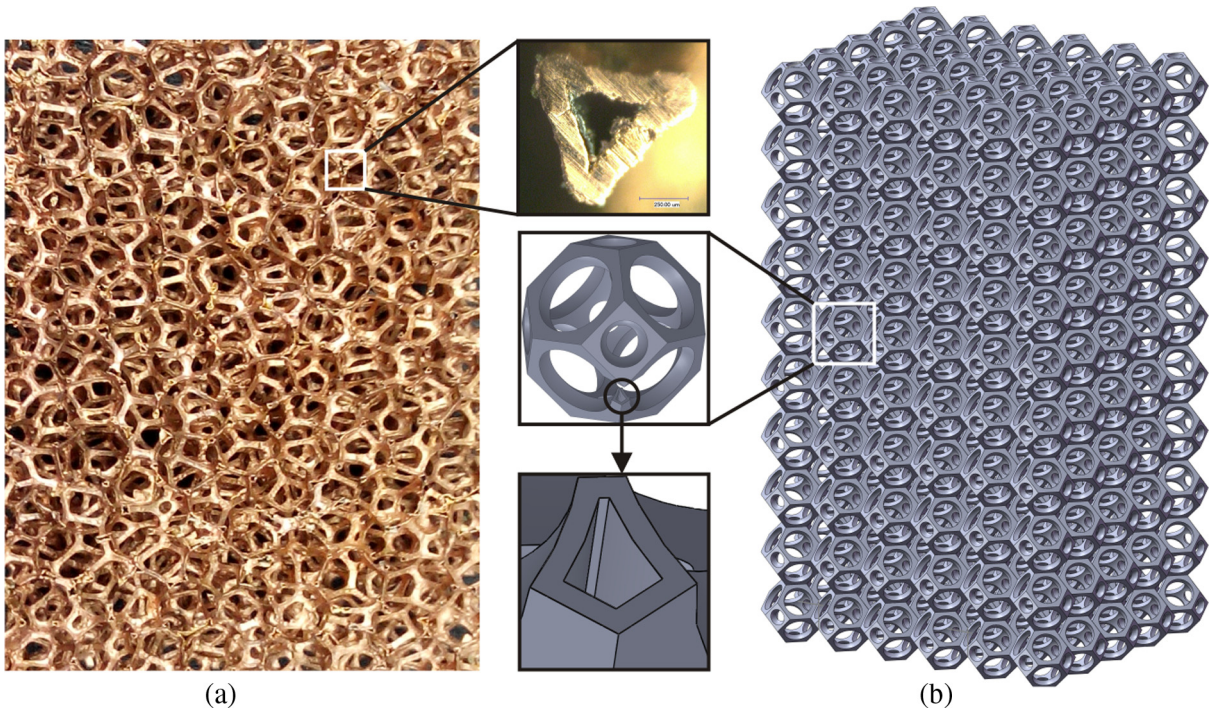


**Fig. 4.** (a) Open-cell copper foam fabricated via the replication of polymeric path approach and its hollow ligaments and (b) topological reconstruction of periodically-distributed sphere-cut tetrakaidecahedron cells.

$C$ and $S$ were Fluent-defined coefficients, recommended to be very large ($1 \times 10^{15}$) and small ($1 \times 10^{-10}$), respectively, and $f_s$ was the solidification fraction in the PCM. According to the phase change condition, $f_s$ took the form:

$$f_s = \begin{cases} 1 & \text{at } T < T_{\text{solidus}} \quad \text{solid} \\ \frac{T_{\text{liquidus}} - T}{T_{\text{liquidus}} - T_{\text{solidus}}} & \text{at } T_{\text{solidus}} < T < T_{\text{liquidus}} \quad \text{mushy} \\ 0 & \text{at } T > T_{\text{liquidus}} \quad \text{liquid} \end{cases} \tag{13}$$

In the present numerical simulations, water served as the phase change material, thereby yielding a small difference (0.01 °C) between solidus and liquidus temperatures, which was good for numerical stability.

For heat transfer in metallic ligaments, the energy transport was governed by:

$$\rho_s c_{ps} \frac{\partial T_s}{\partial t} = \nabla \cdot (k_s \nabla T_s) \tag{14}$$

Conjugate heat transfer was considered at the interface between PCM and metallic ligaments:

$$T_s = T_f, \; k_s \frac{\partial T_s}{\partial n} = k_f \frac{\partial T_f}{\partial n} \tag{15}$$

Here, $\rho$, $c_p$, $k$ and $L$ were separately the density, specific heat, thermal conductivity and latent heat; $T$ was temperature; $t$ denoted time; subscripts $f$ and $s$ stood for PCM and metallic ligaments.

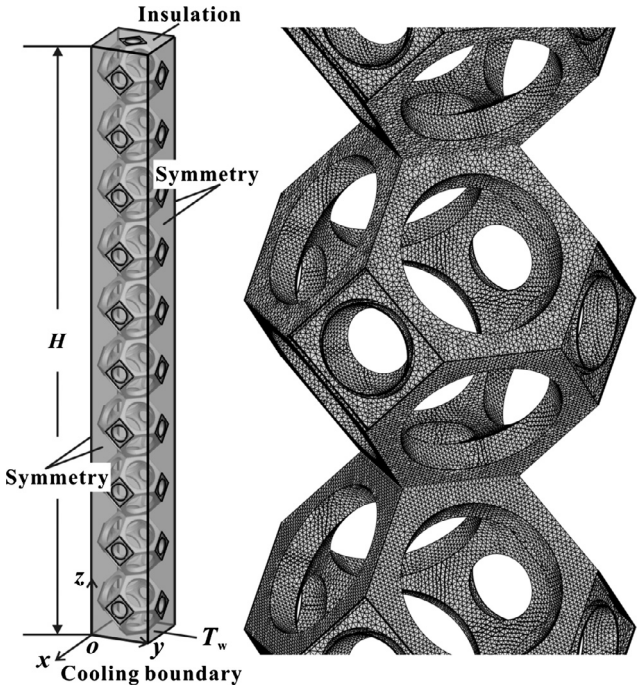


**Fig. 5.** Computational domain with thermal boundaries and representative mesh.

The high resolution scheme was selected for improved computation accuracy and the solution was thought to be converged when the residuals of all the governing equations were less than $10^{-6}$. To check mesh sensitivity, three sets of meshes with 5,652,322, 7,844,953 and 9,568,215 elements were employed. Table 1 compared the predicted parameters of phase change heat transfer at $Ste = 0.22$ and $t = 1000$ s for selected foam with porosity of 0.94 and inner hollow ratio of 0.6. The predicted values from the last two sets of meshes exhibited a deviation less than 1.3%. Hence, the set of mesh having $\sim 7 \times 10^6$ elements was used in subsequent numerical simulations. Validation of the present numerical simulations against experimental measurements was detailed in Section 5.1.

## 4. Experimental facilities

To validate the present analytical model and numerical simulations, a purposely-designed and fabricated test rig was set up, as shown schematically in Fig. 6, consisted mainly of the coolant circulating system, the test section, the data acquisition system for temperature and the snapshot imaging system. The coolant circulating system, which was incorporated with a temperature control unit, a precise pump and compressor, was able to provide a constant temperature boundary for solidification. The whole test section was mainly made up of a transparent Perspex container with size 30 mm (length) × 40 mm (width) × 60 mm (height), where open-cell copper foam saturated with fluid was housed. To guarantee satisfactory thermal insulation for both the side and top walls of the container, polyurethane (PU) foam with thermal conductivity 0.02 W m$^{-1}$ K$^{-1}$ was pasted on the Perspex walls ($k \sim 0.2$ W m$^{-1}$ K$^{-1}$). To further reduce the heat loss from side walls (PU foams) to ambient environment, a big Perspex chamber was facilitated. Two thermocouples were pasted inside and outside the container wall, so that heat loss from the wide walls could be estimated through Fourier's conduction law $Q_{loss} = k_p A(T_{s1} - T_{s2})$. $k_p$ and $A$ were the thermal conductivity and side wall area of the container, and $T_{s1}$ and $T_{s2}$were the inside and outside wall temperatures, respectively.

**Table 1**
Phase change heat transfer parameters numerically obtained with different meshes. Except for full solidification time $t_{full}$, bottom heat flux $q_w$ and dimensionless solidification interface $S(t)/H$ were both obtained at $Ste = 0.22$ and $t = 1000$ s for open-cell copper foam with porosity 0.94 and inner hollow ratio 0.6.

| Parameter | Number of elements used | | |
|---|---|---|---|
| | 5,652,322 | 7,844,953 | 9,568,215 |
| $q_w$ | −3398.76 | −3413.65 | −3450.46 |
| $S(t)/H$ | 0.259 | 0.263 | 0.264 |
| $t_{full}$ | 9769.76 | 9800 | 9867.55 |

The experimental procedures were as follows. Initially, close Valve 2 and 3 and open Valve 1 to circulate the coolant inside the refrigerating unit until a desired low temperature was reached. Then, let coolant with low temperature go through the test section (close V1 and open V2 and 3), forming a heat transfer boundary to solidify the fluid saturated in foam. During the whole process of solidification, six T-type thermocouples (Fig. 6) placed on the surface of the cooper plate in the test section and connected to a temperature scanner (Agilent 34970A) monitored its temperature change $T_w(t)$. To capture the transient position of solidification interface, a camera connected to an image acquisition board attached to the computer and placed next to the test cell was employed. Still images of solidification interface (e.g., boundary between ice formed and distilled water) was recorded through an observing window of the test rig. Based on images captured at a given time, the location of solidification interface was quantitatively calculated. When the bottom wall temperature ($T_w$) was lower than the freezing point ($T_m$) of a given fluid, the solidification interface propagated upwardly. Due to configuration of the present test section (i.e., bottom cooling), global natural convection was significantly suppressed, favoring conduction-dominated heat transfer mode.

## 5. Results and discussion

### 5.1. 1Validation of analytical model and numerical simulation

Fig. 7(a) compared the experimentally measured locations of transient solid-liquid phase interface with those numerically simulated at 600 s, 3000 s and 5400 s, respectively, for water saturated in open-cell copper foam with porosity 0.943 ($1 - \rho^* = 0.965$ by weighting the sample) on its center $y$-$z$ plane. For reference, Fig. 7(b) presented the experimental and numerical results of transient solidification thickness for pure distilled water (no insertion of foam matrix). The initial and cooling boundary temperatures were set as 9.8 °C and −7.8° C for both experiments and simulations. The agreement between simulation results and experimental was in general good.

The experimental images of Fig. 7 showed that the solidification interfaces for both pure water and water-foam composite were globally flat, suggesting that global natural convection was indeed significantly suppressed. Further, by inserting a porous metallic matrix into water, the solidification heat transfer was dramatically enhanced, resulting in considerably decreased time for full solidification as shown in Fig. 8. This was mainly attributed to the enhanced conduction capability of water-foam composite due to foam insertion.

As shown in Fig. 8, achieving good agreement with experimental measurements as well as direct numerical simulations, the extended Neumann's model was also validated, favoring thus pore-scale thermal equilibrium between foam ligaments and saturating fluid. More discussions on this important issue were presented in Section 5.3.

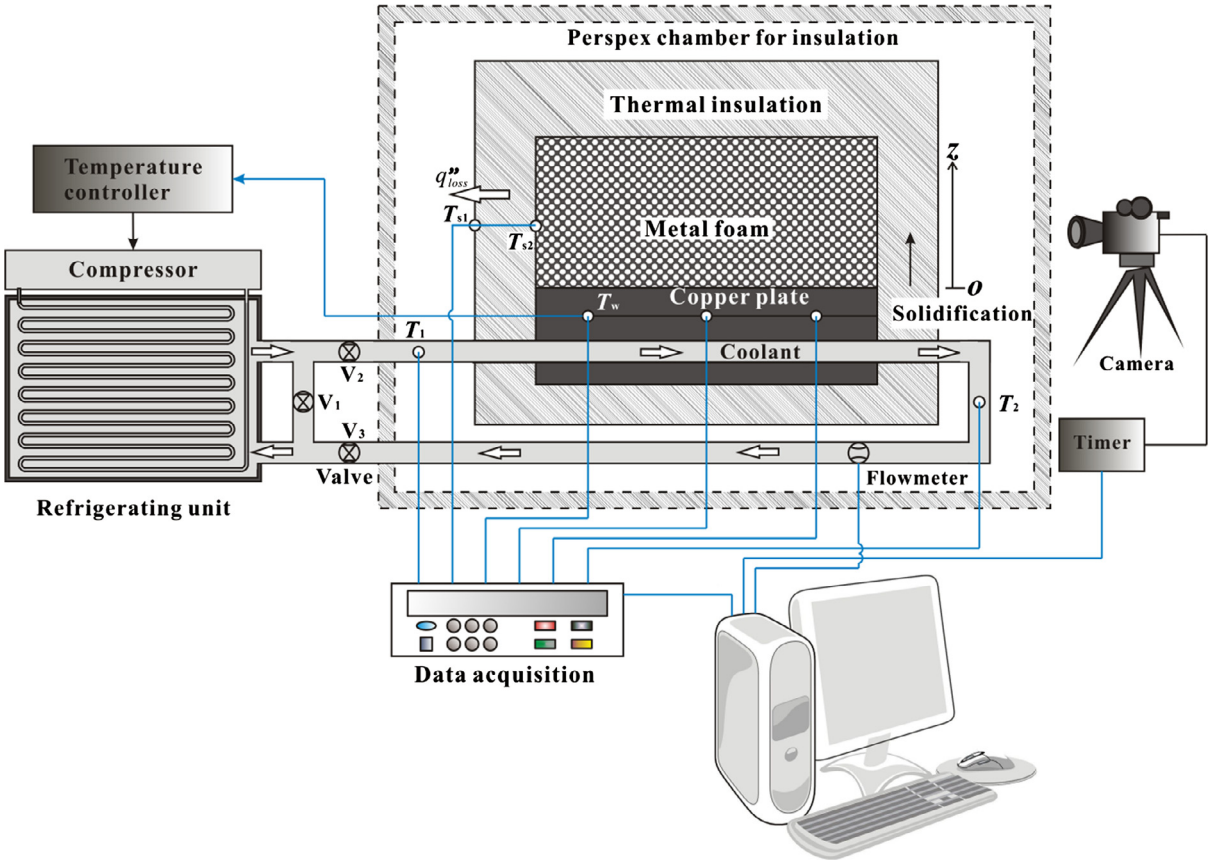


**Fig. 6.** Schematic of experimental setup for solidification heat transfer measurement.

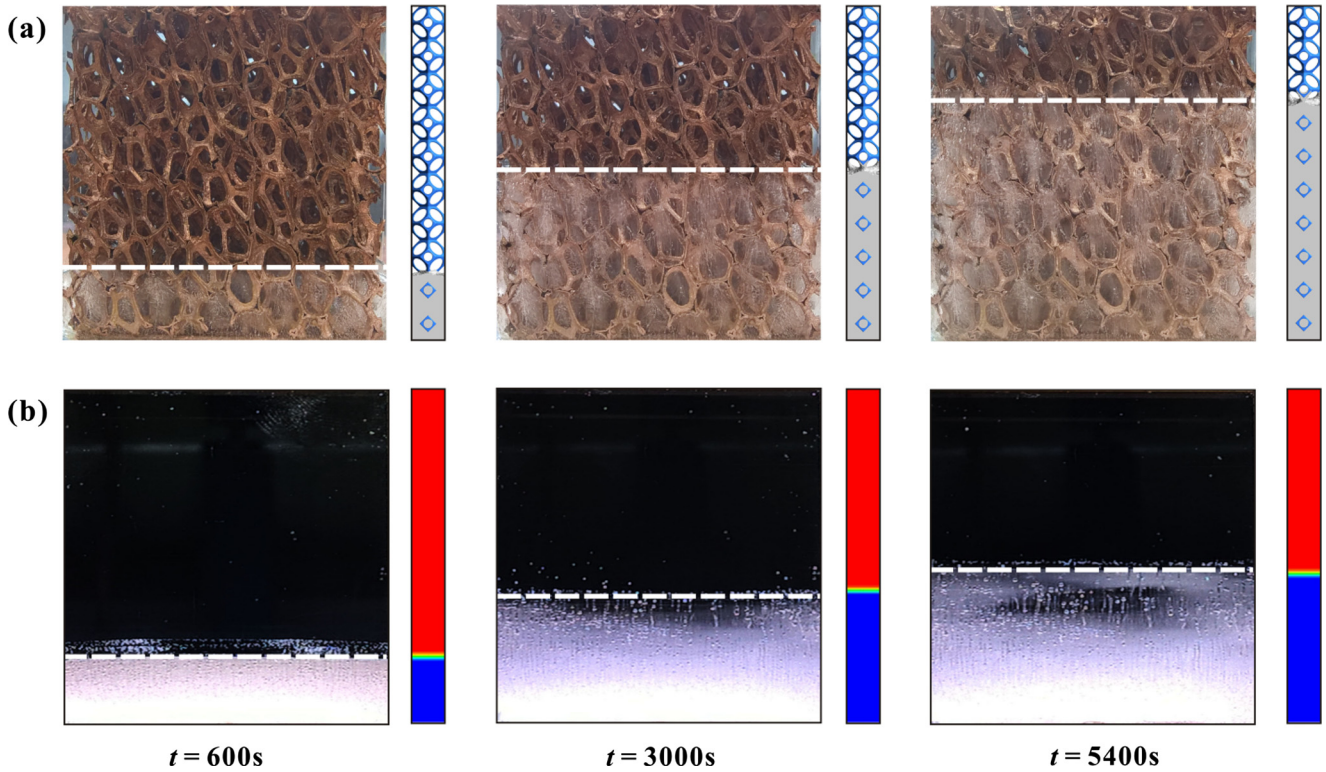


**Fig. 7.** Comparison of transient solidification locations obtained from experiments with those from pore-scale numerical simulations: (a) water-saturated copper foam ($\varepsilon = 0.94$) and (b) pure distilled water.

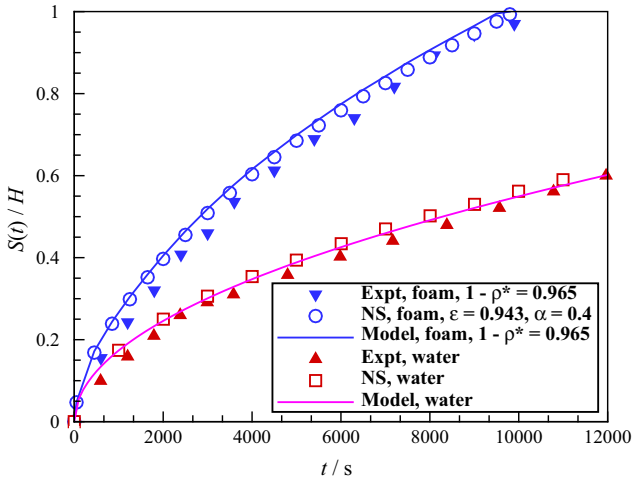


**Fig. 8.** Comparison of dimensionless solidification thickness plotted as a function of time for distilled water and water-saturated porous foam: experiment, numerical simulation and analytical modeling.

### 5.2. Transient location of phase change interface

For the present cooling condition and foam configuration, heat was removed from the bottom so that global natural convection in the liquid phase played a negligible role. As heat transfer in the fluid-foam composite was dominated by heat conduction, globally flat and 1D phase interface (e.g., snapshot of transient phase interface shown in Fig. 7) was observed. From the pore-scale point of view, however, the solidification interface should be characterized microscopically, especially that in the vicinity of metallic ligaments.

Fig. 9 displayed a series of numerically simulated solidification interfaces for water saturated in open-cell copper foam with a fixed porosity of 0.9 but varying inner hollow ratios. At the pore scale, the solidification interface was uneven rather than flat as observed macroscopically in experiments. A large portion of the fluid next to colder metallic ligaments was solidified, forming a local ice cover on the ligaments (Fig. 9). However, only the fluid adjacent to global solidification interface was solidified, i.e., no ice cover was found on ligaments above the solidification interface along the *z*-axis. This phenomenon was distinct from fin-enhanced phase change heat transfer: a large portion of fluid was solidified along the fin surface, observed either microscopically or macroscopically.

The numerically simulated evolution of dimensionless solidification thickness was presented in Fig. 10 for selected porosities and inner hollow ratios. For a given porosity, the inner hollow ratio had a negative effect on phase interface evolution: increasing the hollow ratio delayed interface propagation. For instance, compared with foams with solid ligaments, the full solidification time was increased by 38% and 75% when the foam (porosity fixed at 0.94) had an inner hollow ratio of 0.6 and 0.4, respectively. On the other hand, with the inner hollow ratio fixed at 0.4, the full solidification time was increased by 11% and 27% if the foam porosity was increased from 0.90 to 0.92 and 0.94, respectively.

The delayed solidification of water saturated in open-cell metallic foam with either high porosity or inner hollow ratio was mainly caused by the decreased effective thermal conductivity of the foam. As foam porosity or inner hollow ratio was increased, the effective conductivity was reduced. The two parameters might be integrated into one parameter (i.e., foam relative density) as shown in Eq. (8). Therefore, the foam relative density might be the dominating pore parameter for phase change heat transfer in PCM-foam composites.

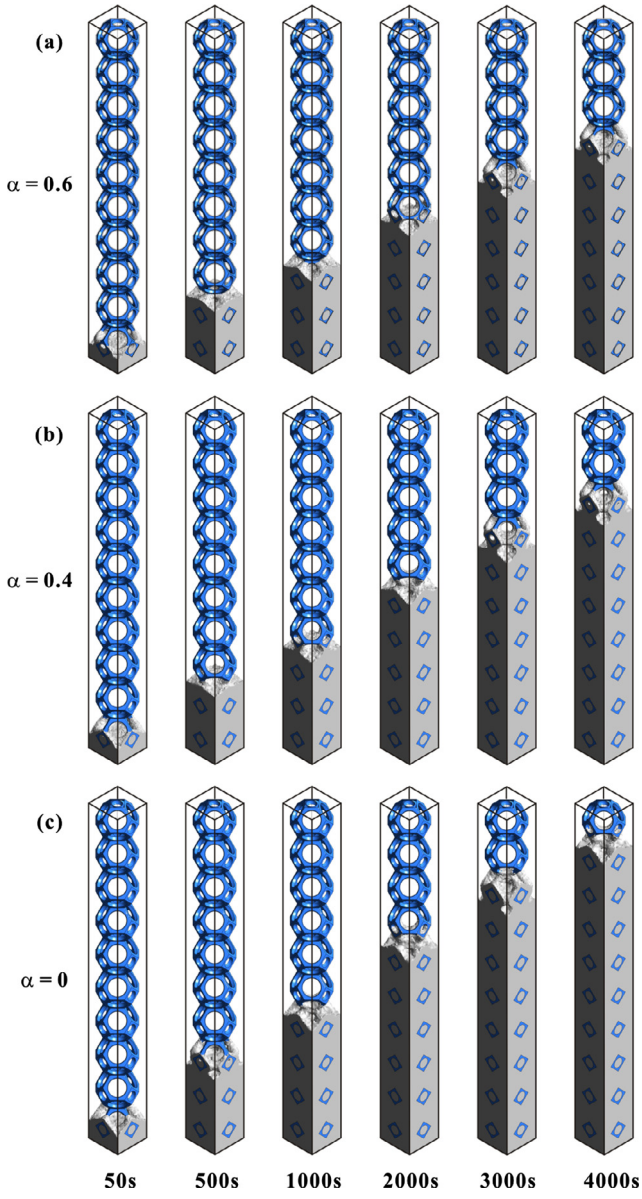


**Fig. 9.** Snapshots of transient solidification location obtained from pore-scale numerical simulations with a given porosity of 0.9 but different inner hollow ratios: (a) $\alpha = 0.6$; (b) $\alpha = 0.4$; and (c) $\alpha = 0$.

Fig. 11 presented the evolution of dimensionless solidification thickness for foams having the same relative density of 0.034 but different porosities and inner hollow ratios. The transient solidification location collapsed with each other, confirming the dominant role of foam relative density in phase change heat transfer. From the images shown in Figs. 3(a) and 4(a), it was seen that although the ligaments were hollow, the overall topological features of the foam had not been changed by the RPP fabrication approach. As a result, as long as the porosity remained unchanged, the flow resistance of the foam would not change even if its relative density was varied.

Typically, when open-cell metallic foams were used to enhance forced convection or chemical reaction, a series of pore parameters should be characterized, such as porosity, pore density, inner hollow ratio and relative density. Often, the quantification of these parameters needed complicated measuring procedures and equipment. For phase change heat transfer, however, the foam relative density as a key parameter could be readily determined

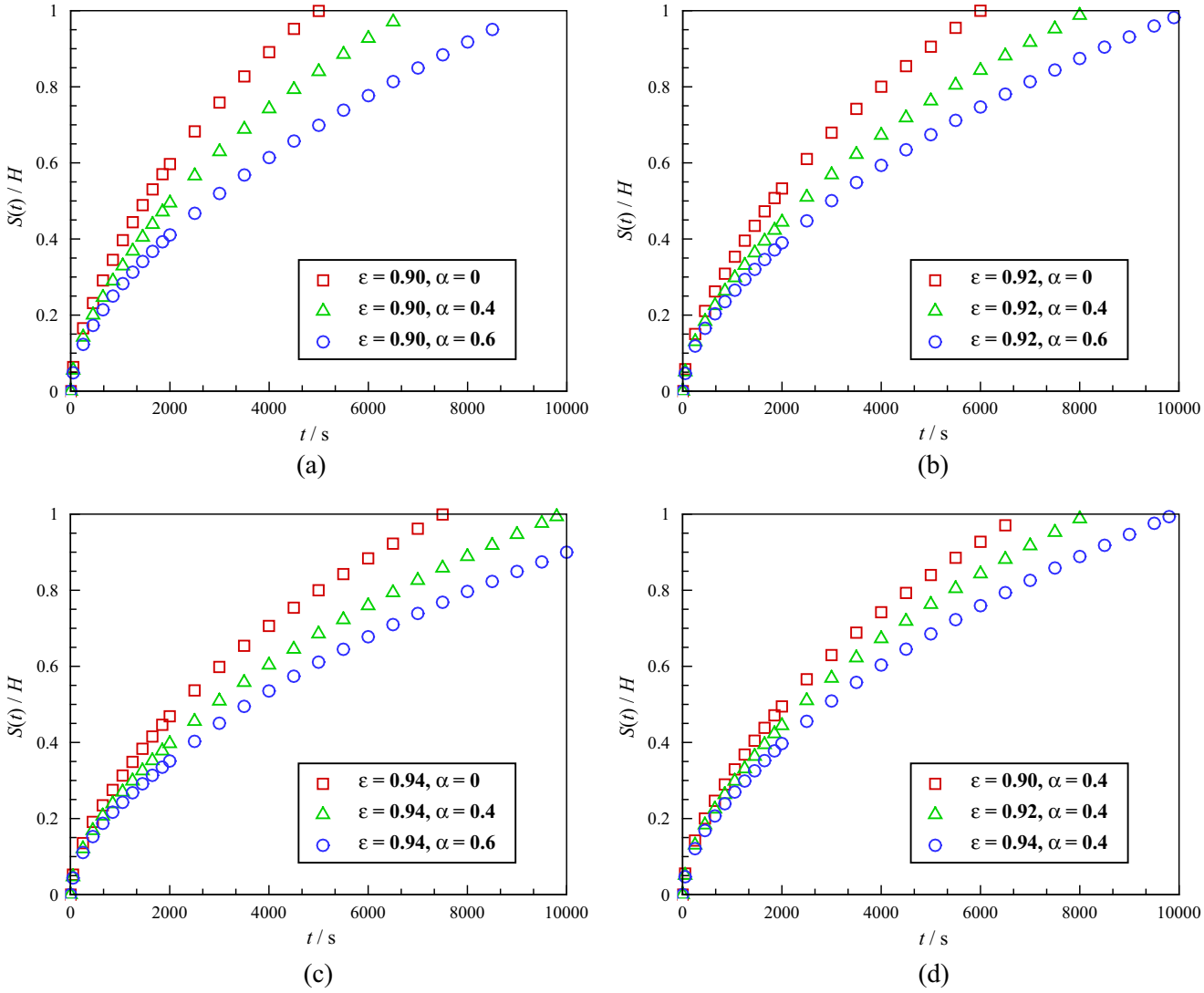


**Fig. 10.** Dimensionless solidification thickness for fluid saturated in open-cell metal foam having different inner hollow ratios: (a) $\varepsilon = 0.9$, $\alpha = 0, 0.4, 0.6$; (b) $\varepsilon = 0.92$, $\alpha = 0, 0.4, 0.6$; (c) $\varepsilon = 0.94$, $\alpha = 0, 0.4, 0.6$; and (d) $\alpha = 0.4$, $\varepsilon = 0.9, 0.92, 0.94$.

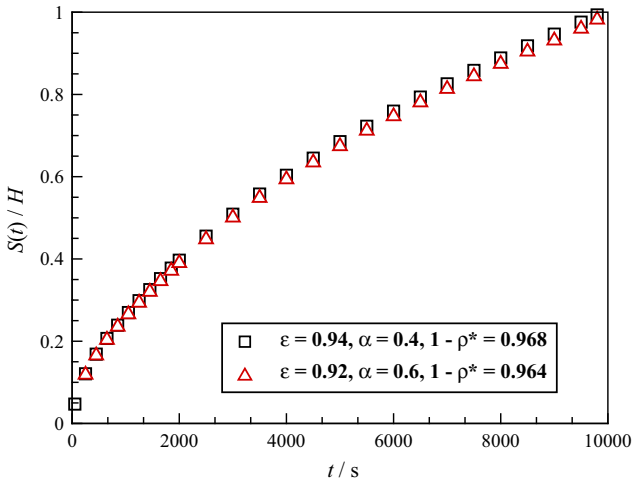


**Fig. 11.** Dimensionless solidification thickness plotted as a function of time for two open-cell foams having identical relative density but different porosities.

by weighing the sample, thus convenient for engineering applications of cold storage.

### 5.3. Local thermal equilibrium

In Section 5.2, it was demonstrated that the solidification interface was microscopically circuitous and a large portion of fluid adjacent metallic ligaments was solidified. This phase change phenomenon could be explained by analyzing local temperature distribution in both the PCM and metallic ligaments, as shown in Fig. 12 (a) for foams with varying porosities (0.9, 0.92, 0.94) and fixed inner hollow ratio (0.6).

The simulated temperature field of Fig. 12(a) demonstrated that the temperature difference between metallic ligaments and saturating PCM was quite small, revealing a local thermal equilibrium state. Quantitatively, the temperature difference between PCM and metallic ligaments during the whole solidification process was depicted in Fig. 12(b), where the temperatures were calculated based on integral averaged value over the entire slice. There seemed to be no temperature difference, except the two peaks, i.e., 0.37 and 0.29 °C at 300 s and 2850 s when phase change

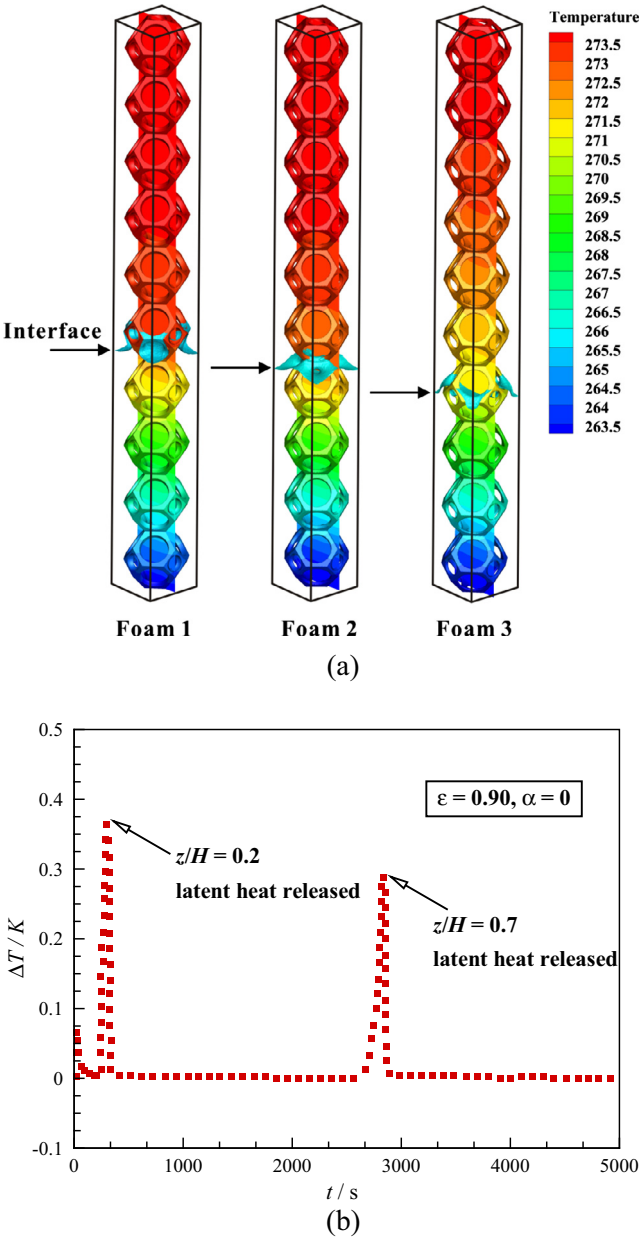


**Fig. 12.** (a) Simulated temperature distribution in PCM and foam ligaments at 2000s for foam 1 (porosity 0.90), foam 2 (0.92) and foam 3 (0.94) with fixed inner hollow ratio of 0.6; and (b) temperature difference between PCM and foam ligaments plotted as a function of time for open-cell foam with solid ligaments ($\alpha = 0$) and fixed porosity 0.90.

occurred at $z/H = 0.2$ and 0.7. This explained why local solidification interface was not flat at pore scale. Once the porous foam was inserted, heat was transferred much faster and more efficiently, so that the temperature of fluid adjacent the metallic ligaments became lower than that in the pore center. In addition, upon increasing the foam porosity or inner hollow ratio, the peak value was dropped and less fluid was solidified due to the reduced thermal conduction capability of foam.

In the present study, the two small peaks were found at $Ste = 0.22$. Consequently, local thermal equilibrium at pore scale held so that the one-equation model could be employed to predict phase change heat transfer for fluid saturated in open-cell metallic foams. Similarly, the modified Neumann solution could be exploited as well. Nonetheless, as the *Ste* number was increased to say 0.75, the peak value was significantly increased to 1.7 and 1.25 °C. Under such conditions, it was necessary to consider local thermal non-equilibrium during volume averaging, as discussed in Hu and Patnaik [34].

During solidification, an open-cell metallic foam matrix played two roles: (i) for the solidified part, the presence of foam improved the effective thermal conductivity of ice-foam composite, enabling a higher efficiency of cold (sensible heat) removal from the cooling boundary for further solidification and (ii) for the liquid part, metallic ligaments helped to conduct the sensible heat for both the liquid phase and metallic ligaments and transported the latent heat released by the newly-formed ice. When local thermal equilibrium at pore scale was applicable, the ligaments shared the same temperature with the saturating fluid within a pore, indicating that the first role of foam was more important for enhanced phase change heat transfer.

### 5.4. Bottom surface heat flux

Fig. 13 depicted the area-weighted average surface heat flux on the bottom of the computational domain. The bottom surface heat flux decreased with time elapsed under constant temperature cooling boundary, with its highest value found at the initial stage (due to latent heat released in the vicinity of the boundary). With solidification layer thickening, the phase interface propagated further away from the bottom wall. At a given porosity, increasing the ligament hollow ratio decreased the bottom heat flux; so did porosity for a given hollow ratio. This was mainly attributed to the reduction in contact area caused by increased inner hollow ratio or porosity. Besides, the inner hollow ratio was seen to have a more obvious effect on bottom heat flux than porosity. Fig. 14(a) compared the ratio of bottom heat flux on metallic ligaments to that on PCM. The heat flux ratio decreased as the inner hollow ratio was increased. A 49 times higher increment in bottom heat flux was found by inserting foam with a porosity of 0.90 into PCM, and the increment remained significant when the inner hollow ratio was 0.6.

To facilitate quantitative comparison of the influence of inner hollow ratio on phase change heat transfer, a heat transfer coefficient averaged over the entire solidification process was introduced by Feng et al. [36], expressed as:

$$\bar{h} = \frac{\int_0^{t_{\text{full}}} q_w \mathrm{d}t}{t_{\text{full}}(T_i - T_w)} \tag{16}$$

where $\bar{h}$ was the averaged heat transfer coefficient, $q_w$ was the bottom heat flux, $t_{\text{full}}$ was the full solidification time, and $T_i$ and $T_w$ were the temperatures of initial state and cooling boundary, respectively. When the averaged heat transfer coefficient was plotted as a function of inner hollow ratio, a similar variation trend was observed as shown in Fig. 14(b): the foam with lowest porosity and inner hollow ratio exhibited the highest heat transfer coefficient. It was also observed that there was little difference in averaged heat transfer coefficient between foams with ($\varepsilon = 0.92$, $\alpha = 0.6$) and ($\varepsilon = 0.94$, $\alpha = 0.4$), consistent with the result of Fig. 11 that the transient solidification location collapsed for these two foams. This finding supported a phase change heat transfer enhancement strategy by increasing the effective thermal conductivity of PCM-foam composite layer adjacent the cooling boundary (i.e., increasing the bottom heat flux to increase averaged heat transfer coefficient).

### 5.5. Effect of local natural convection on solidification

In general, the effect of global natural convection upon phase change process such as solidification was neglected as bottom cooling or top heating was commonly used in experimental

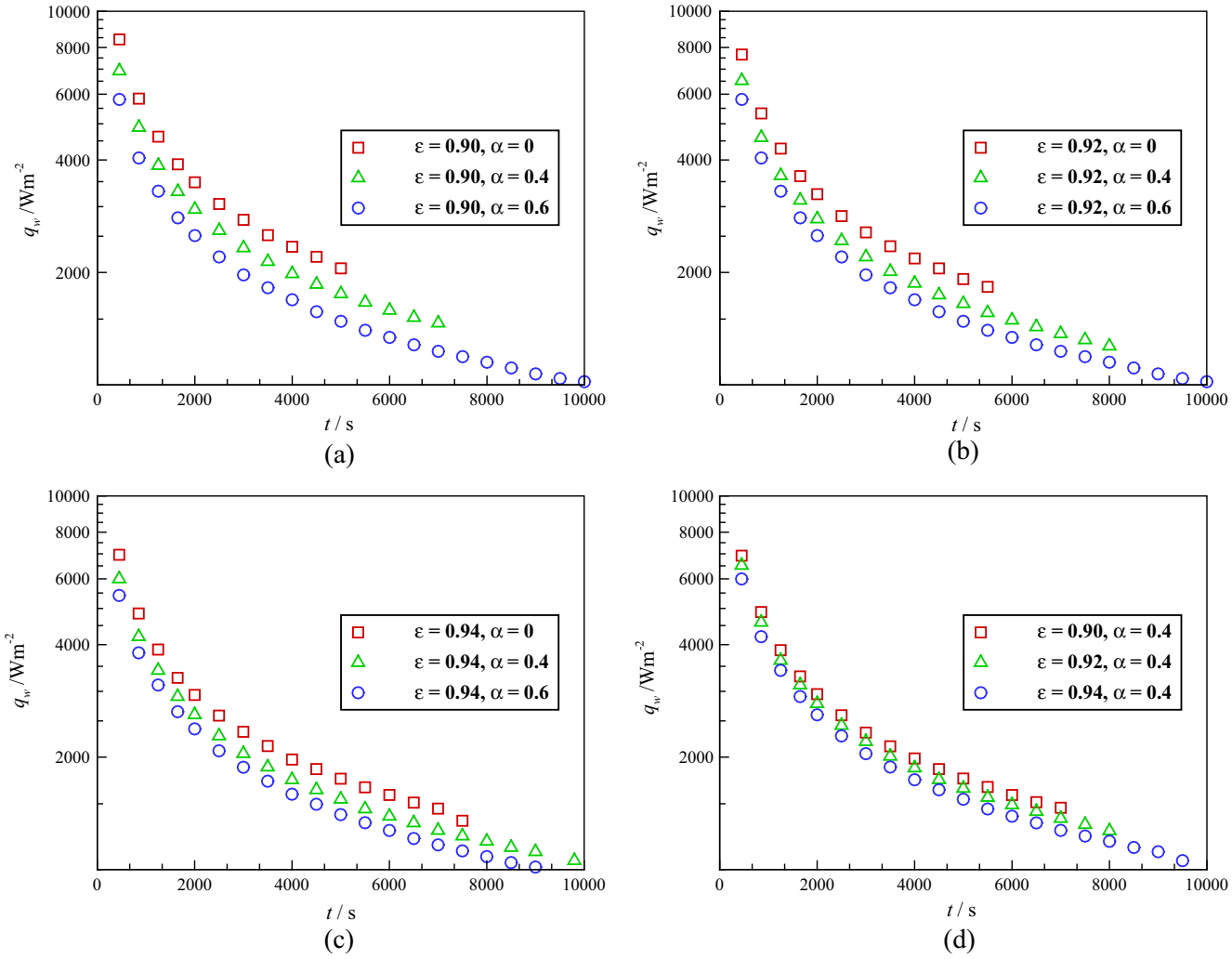


**Fig. 13.** Bottom heat flux plotted as a function of time for fluid saturated in open-cell metal foams with different inner hollow ratios: (a) $\varepsilon = 0.9$, $\alpha = 0$, 0.4, 0.6; (b) $\varepsilon = 0.92$, $\alpha = 0$, 0.4, 0.6; (c) $\varepsilon = 0.94$, $\alpha = 0$, 0.4, 0.6; and (d) $\alpha = 0.4$, $\varepsilon = 0.9$, 0.92, 0.94.

measurements and volume-averaged numerical simulations. However, how to observe local natural convection at pore scale and quantify its contribution to evolution of overall solidification interface remained elusive. In the present study, to address this issue, the Boussinesq assumption was adopted to simulate local fluid convection in PCM-foam composite, yielding the results shown in Fig. 15 for transient phase interface. With local natural convection accounted for, the solid-liquid phase interface front was similar to that obtained for the conduction dominated case (i.e., effect of natural convection neglected). Although natural convection did exist in the liquid layer (velocity slices in Fig. 15), the fluid velocity was negligibly small ($\sim 10^{-5}$ m/s), suggesting that local natural convection contributed little to solidification. This was further supported by the results of Fig. 8, i.e., the full numerical simulation result obtained by accounting for both the conduction and convection was only 5% percent higher than the analytical model prediction (conduction only).

### 5.6. Applicability analysis

Amongst various porous media, open-cell metal foams exhibit distinctive properties: relatively low manufacturing cost, ultra-low density, moderate stiffness and strength, and high surface area-to-volume ratio. The particularly high surface area-to-volume ratio (2000–8000 m$^2$/m$^3$), strong flow mixing capability and high conducting metallic ligaments pave the foundation for applying open-cell metal foam to the heat transfer enhancement for various heat exchangers. Metal foam can be cut into pieces via wire-electrode cutting and can be weld with heat transfer surfaces. The quality of cutting and welding can be well controlled according to the present manufacturing technology (see Fig. 1).

To evaluate the cost-effective for metal-foam-cored heat exchanger for cold storage, the initial investment and lifetime cost should be quantified. With involving metal foam, the initial investment for fabricating a phase change heat exchanger is apparently increased, compared with the original plate heat exchanger. The increment is mainly consisted of the material cost for metal foam and welding cost. According to the manufacturers, the price of metal foam is 770 US dollars per cubic meter. A typical plate heat exchanger has a total void volume of 12 m$^3$. Therefore, the cost for metal foam can be estimated to be 9240 dollars. The welding cost is estimated to be 5% of the total material cost, and thus the increment of the total initial investment for metal-foam-cored heat exchanger is 9702 dollars, compared with the original plate heat exchanger.

Now we will compare the lifetime cost for the system with and without metal foam. Suppose that the refrigerant for the ice-making system is R134a; the Coefficient of Performance (COP)

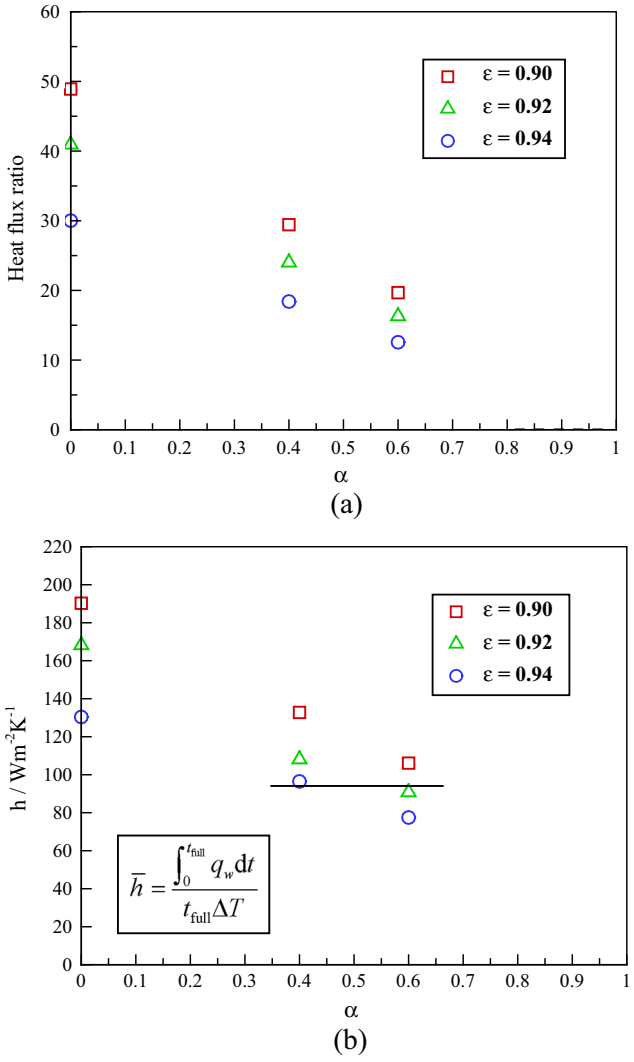


**Fig. 14.** (a) Ratio of bottom heat flux on foam ligament to that on PCM and (b) influence of foam porosity on average heat transfer coefficient.

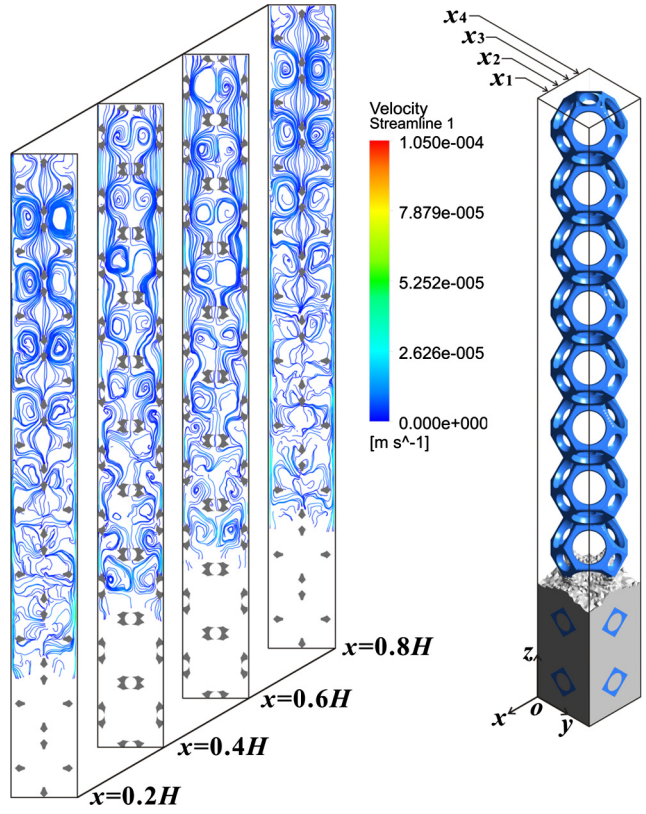


**Fig. 15.** Snapshots of numerically simulated transient solidification interface with local natural convection considered.

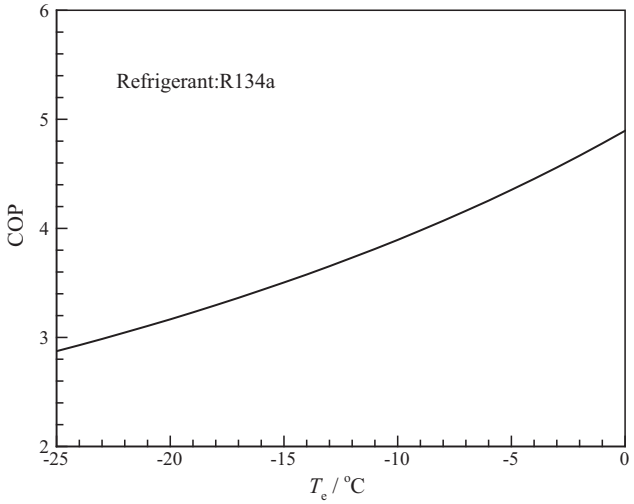


**Fig. 16.** Coefficient of performance (COP) curve as a function of evaporating temperature for a typical refrigeration system using R134a as the refrigerant.

curve as a function of evaporating temperature ($T_e$) for this refrigeration system is depicted in Fig. 16. It can be observed that COP is increased with the evaporating temperature, indicating that a higher evaporating temperature results in higher energy efficiency. The involvement of metal foam can significantly reduce the full solidification time under the same constant wall temperature ($T_w$). On the other hand, if the full solidification time is fixed for the heat exchanger with/without employing metal foam, the boundary wall temperature of the case with metal foam will be higher than that without foam. In this study, the boundary wall temperature ($T_w$) equals to the evaporating temperature ($T_e$), indicating that the COP of the ice-making system is improved by using metal foam as heat transfer enhancement. An example as shown in Table 2 is analyzed here to address the lifetime cost with metal foam involved. For the same initial temperature of water (12.4 °C), the boundary wall temperature is increased from −8.4 °C to −3.6 °C and the COP is increased from 4.0–4.5 when metal foam is employed. Accordingly, a considerable amount of electricity (31.22 kW h) is saved per night. The cooling load of countries, e.g. Singapore in tropical climate is very high. When applying the metal-foam-cored phase change heat exchanger, 2139 US dollars will be saved per year (the electricity price at night is 0.188 dollars). Therefore, as for a single metal-foam-cored heat exchanger, a period of 4.5 years is needed to recoup the costs of initial investment for fabricating the heat exchanger. For a 30-year lifetime, the metal-foam-cored plate heat exchanger can save about 56,683 dollars, in comparison with plate heat exchanger. This indicates the economic applicability of metal foam as heat transfer enhancement.

**Table 2**
Comparison of electricity consumption per night for phase change heat exchanger with/without metal foam as heat transfer enhancement.

| Heat exchanger type | $T_i$/°C | $T_w$/°C | COP | Electricity consumption per night/kW h |
|---|---|---|---|---|
| Plate heat exchanger | 12.4 | −8.4 | 4.0 | 280.92 |
| Metal-foam-cored | 12.4 | −3.6 | 4.5 | 249.71 |

## 6. Conclusions

Solidification features of PCM saturated in open-cell metallic foams were investigated analytically, numerically and experimentally. Based on the local thermal equilibrium assumption and the volume-averaging theory, an extension to Neumann's classical solution was made to predict the phase interface evolution. With periodically distributed reconstructed tetrakaidecahedron cells employed to mimic the cellular morphology of open-ell foam, direct 3D numerical simulations of solidification in the PCM-foam composite were carried out. To validate analytical prediction and numerical simulation, solidification heat transfer was measured for both pure water and water-foam composites, with open-cell copper foams fabricated via the replication of polymeric path (RPP) route employed. Good agreement between experimental measurements and analytical/numerical predictions were achieved. The main conclusions were drawn as follows:

(1) Open-cell metal foams exhibited promising potential for phase change heat transfer enhancement. The full solidification time could be reduced by ~3 times by inserting a foam matrix (porosity 0.90) into water, due mainly to significantly increased heat conduction by metallic ligaments.
(2) At a given porosity, solidification was retarded when foams with hollow ligaments (i.e., fabricated via the RPP route) were adopted. The retardant effect was more obvious for foams having higher inner hollow ratios, due to reduction in averaged heat transfer coefficient for PCM-foam composites.
(3) Transient solidification curves for foams having different porosities and ligament inner hollow ratios but identical relative density collapsed, as the averaged heat transfer coefficient at pore scale remained unchanged. Combining porosity and ligament inner hollow ratio, the relative density appeared to be a dominant morphological parameter for characterizing phase change heat transfer in PCM-foam composites.
(4) Temperature difference between saturating PCM and metallic ligaments was observed only during a short period of time when phase change was initiated. For low *Ste* numbers (e.g., 0.22), local thermal equilibrium held and the simple one-equation model was applicable.
(5) Based on pore-scale direct numerical simulations, negligible effects of both global and local natural convection on phase change heat transfer in PCM-foam composites with bottom cooling were observed.
(6) For the same initial temperature of water (12.4 °C), the boundary wall temperature is increased from −8.4 °C to −3.6 °C and the COP is increased from 4.0 to 4.5 when metal foam is employed. For a 30-year lifetime in Singapore, the metal-foam-cored plate heat exchanger can save a considerable amount of operating cost (56,683 dollars), in comparison with plate heat exchanger.

## Acknowledgement

This work was supported by the National Natural Science Foundation of China (51506160), China Post-doctoral Science Foundation Funded Project (2015M580845, 2016T90916), and the Beijing Key Lab of Heating, Gas Supply, Ventilating and Air Conditioning Engineering (NR2015K08 & NR2016K01).

## References

[1] Chang CC. A multivariate causality test of carbon dioxide emissions, energy use and economic growth in China. Appl Energy 2010;87:3533–7.
[2] Govindaraju VGRC, Tang CF. The dynamic links between $CO_2$ emissions, economic growth and coal consumption in China and India. Appl Energy 2013;104:310–8.
[3] Sharma SS. Determinants of carbon dioxide emissions: empirical evidence from 69 countries. Appl Energy 2011;88:376–82.
[4] Liu W, Lund H, Mathiesen BV, Zhang X. Potential of renewable energy systems in China. Appl Energy 2011;88:518–25.
[5] Wang K, Wei YM, Zhang X. Energy and emissions efficiency patterns of Chinese regions: a multi-directional efficiency analysis. Appl Energy 2013;104:105–16.
[6] Pérez-Lombard L, Ortiz J, Pout C. A review on buildings energy consumption information. Energy Build 2008;40:394–8.
[7] Hu Y, Yan J. Characterization of flue gas in oxy-coal combustion processes for $CO_2$ capture. Appl Energy 2012;90:113–21.
[8] Tian Y, Zhao L, Meng H, Sun L, Yan J. Estimation of un-used land potential for biofuels development in (the) People's Republic of China. Appl Energy 2009;86:S77–85.
[9] Chua K, Chou S, Yang W, Yan J. Achieving better energy-efficient air conditioning–a review of technologies and strategies. Appl Energy 2013;104:87–104.
[10] Zhou D, Zhao C-Y, Tian Y. Review on thermal energy storage with phase change materials (PCMs) in building applications. Appl Energy 2012;92:593–605.
[11] Oró E, de Gracia A, Castell A, Farid M, Cabeza L. Review on phase change materials (PCMs) for cold thermal energy storage applications. Appl Energy 2012;99:513–33.
[12] Wang L, Meng D. Fatty acid eutectic/polymethyl methacrylate composite as form-stable phase change material for thermal energy storage. Appl Energy 2010;87:2660–5.
[13] Hawlader M, Uddin M, Khin MM. Microencapsulated PCM thermal-energy storage system. Appl Energy 2003;74:195–202.
[14] Wang W, Yang X, Fang Y, Ding J, Yan J. Enhanced thermal conductivity and thermal performance of form-stable composite phase change materials by using β-Aluminum nitride. Appl Energy 2009;86:1196–200.
[15] Xiao X, Zhang P, Li M. Preparation and thermal characterization of paraffin/metal foam composite phase change material. Appl Energy 2013;112:1357–66.
[16] Yang XH, Lu TJ, Kim T. Temperature effects on the effective thermal conductivity of phase change materials with two distinctive phases. Int Comm Heat Mass Trans 2011;38:1344–8.
[17] Tian Y, Zhao C-Y. A review of solar collectors and thermal energy storage in solar thermal applications. Appl Energy 2013;104:538–53.
[18] Zhang P, Meng ZN, Zhu H, Wang YL, Peng SP. Melting heat transfer characteristics of a composite phase change material fabricated by paraffin and metal foam. Appl Energy 2017;185(Part 2):1971–83.
[19] Yang XH, Wang WB, Yang C, Jin LW, Lu TJ. Solidification of fluid saturated in open-cell metallic foams with graded morphologies. Int J Heat Mass Transf 2016;98:60–9.
[20] Wang P, Liu D, Xu C. Numerical study of heat transfer enhancement in the receiver tube of direct steam generation with parabolic trough by inserting metal foams. Appl Energy 2013;102:449–60.
[21] Zhang Z, Zhang N, Peng J, Fang X, Gao X, Fang Y. Preparation and thermal energy storage properties of paraffin/expanded graphite composite phase change material. Appl Energy 2012;91:426–31.
[22] Liu Z, Yao Y, Wu H. Numerical modeling for solid-liquid phase change phenomena in porous media: shell-and-tube type latent heat thermal energy storage. Appl Energy 2013;112:1222–32.
[23] Mahmoud S, Tang A, Toh C, Raya AD, Soo SL. Experimental investigation of inserts configurations and PCM type on the thermal performance of PCM based heat sinks. Appl Energy 2013;112:1349–56.
[24] ERG Aerospace Corporation. Duocel Aluminum foam <http://www.ergaerospace.com/index.html>.
[25] Siahpush A, O'Brien J, Crepeau J. Phase change heat transfer enhancement using copper porous foam. J Heat Transf 2008;130:082301.
[26] Feng SS, Zhang Y, Shi M, Wen T, Lu TJ. Unidirectional freezing of phase change materials saturated in open-cell metal foams. Appl Therm Eng 2015;88:315–21.

[27] Tong X, Khan JA, Ruhul M. Enhancement of heat transfer by inserting a metal matrix into a phase change material. Numer Heat Transf Part A Appl 1996;30:125–41.
[28] Li WQ, Qu ZG, He YL, Tao WQ. Experimental and numerical studies on melting phase change heat transfer in open-cell metallic foams filled with paraffin. Appl Therm Eng 2012;37:1–9.
[29] Mesalhy O, Lafdi K, Elgafy A, Bowman K. Numerical study for enhancing the thermal conductivity of phase change material (PCM) storage using high thermal conductivity porous matrix. Energy Convers Manage 2005;46:847–67.
[30] Yang Z, Garimella SV. Melting of phase change materials with volume change in metal foams. J Heat Transf 2010;132:062301.
[31] Tian Y, Zhao CY. A numerical investigation of heat transfer in phase change materials (PCMs) embedded in porous metals. Energy 2011;36:5539–46.
[32] Srivatsa PVSS, Baby R, Balaji C. Numerical investigation of PCM based heat sinks with embedded metal foam/crossed plate fins. Numer Heat Transf Part A Appl 2014;66:1131–53.
[33] Fleming E, Wen SY, Shi L, da Silva AK. Experimental and theoretical analysis of an aluminum foam enhanced phase change thermal storage unit. Int J Heat Mass Transf 2015;82:273–81.
[34] Hu X, Patnaik SS. Modeling phase change material in micro-foam under constant temperature condition. Int J Heat Mass Transf 2014;68:677–82.
[35] Hu X, Wan H, Patnaik SS. Numerical modeling of heat transfer in open-cell micro-foam with phase change material. Int J Heat Mass Transf 2015;88:617–26.
[36] Feng SS, Shi M, Li Y, Lu TJ. Pore-scale and volume-averaged numerical simulations of melting phase change heat transfer in finned metal foam. Int J Heat Mass Transf 2015;90:838–47.
[37] Carslaw HS, Jaeger JC. Conduction of heat in solids. 2nd ed. Oxford: Clarendon Press; 1959.
[38] Yang XH, Lu TJ, Kim T. An analytical model for permeability of isotropic porous media. Phys Lett A 2014;378:2308–11.
[39] Yang XH, Kuang JJ, Lu TJ, Han FS, Kim T. A simplistic analytical unit cell based model for the effective thermal conductivity of high porosity open-cell metal foams. J Phys D-Appl Phys 2013;46:255302.
[40] Yang XH, Bai JX, Yan HB, Kuang JJ, Lu TJ, Kim T. An analytical unit cell model for the effective thermal conductivity of high porosity open-cell metal foams. Transp Porous Med 2014;102:403–26.
[41] Boomsma K, Poulikakos D. On the effective thermal conductivity of a three-dimensionally structured fluid-saturated metal foam. Int J Heat Mass Transf 2001;44:827–36.
[42] Weaire DL, Hutzler S. The physics of foams. Oxford University Press; 2001.
[43] ANSYS fluent software package: user's manual, 14.5; 2012.